



This is a repository copy of *Nanoscopic characterisation of individual endogenous protein aggregates in human neuronal cells*.

White Rose Research Online URL for this paper:

<https://eprints.whiterose.ac.uk/160179/>

Version: Published Version

Article:

Whiten, D.R., Zuo, Y., Calo, L. et al. (14 more authors) (2018) Nanoscopic characterisation of individual endogenous protein aggregates in human neuronal cells. *ChemBioChem*, 19 (19). pp. 2033-2038. ISSN 1439-4227

<https://doi.org/10.1002/cbic.201800209>

Reuse

This article is distributed under the terms of the Creative Commons Attribution (CC BY) licence. This licence allows you to distribute, remix, tweak, and build upon the work, even commercially, as long as you credit the authors for the original work. More information and the full terms of the licence here:

<https://creativecommons.org/licenses/>

Takedown

If you consider content in White Rose Research Online to be in breach of UK law, please notify us by emailing eprints@whiterose.ac.uk including the URL of the record and the reason for the withdrawal request.



eprints@whiterose.ac.uk
<https://eprints.whiterose.ac.uk/>



Nanoscopic Characterisation of Individual Endogenous Protein Aggregates in Human Neuronal Cells

Daniel R. Whiten^{+, [a]}, Yukun Zuo^{+, [a]}, Laura Calo,^[c] Minee-Liane Choi,^[d] Suman De,^[a] Patrick Flagmeier,^[a] David C. Wirthensohn,^[a] Franziska Kundel,^[a] Rohan T. Ranasinghe,^[a] Santiago E. Sanchez,^[a] Dilan Athauda,^[d] Steven F. Lee,^[a] Christopher M. Dobson,^[a] Sonia Gandhi,^[d] Maria-Grazia Spillantini,^[c] David Klenerman,^{*, [a, b]} and Mathew H. Horrocks^{*, [a, e, f]}

The aberrant misfolding and subsequent conversion of monomeric protein into amyloid aggregates characterises many neurodegenerative disorders, including Parkinson's and Alzheimer's diseases. These aggregates are highly heterogeneous in structure, generally of low abundance and typically smaller than the diffraction limit of light (≈ 250 nm). To overcome the challenges these characteristics pose to the study of endogenous aggregates formed in cells, we have developed a method to characterise them at the nanometre scale without the need for a conjugated fluorophore. Using a combination of DNA PAINT and an amyloid-specific aptamer, we demonstrate that this technique is able to detect and super-resolve a range of aggregated species, including those formed by α -synuclein and amyloid- β . Additionally, this method enables endogenous protein aggregates within cells to be characterised. We found that neuronal cells derived from patients with Parkinson's disease contain a larger number of protein aggregates than those from healthy controls.

Protein misfolding and aggregation is closely associated with the development of many neurodegenerative disorders, such as Alzheimer's disease (AD) and Parkinson's disease (PD).^[1] In AD, the protein tau is deposited in intracellular inclusions,^[2] while the amyloid beta (A β) peptide is in extracellular plaques. Similarly, in PD, aggregates of the protein α -synuclein (α S) are found in Lewy bodies^[3] within neuronal cells. These proteins are often heavily post-translationally modified, for example, α S undergoes phosphorylation, nitration and truncation,^[4-6] this makes it important to be able to characterise the real endoge-

nous aggregates formed in cells, as these can differ from those formed by unmodified proteins.

Soluble nanometre-sized protein oligomers have been identified as the major cytotoxic species in AD and PD,^[7-10] but the study of such species has remained challenging, as they tend to be low in abundance and adopt a wide range of heterogeneous structures. To overcome this problem, we have developed an array of single-molecule techniques^[11-14] to observe oligomeric species individually, and have applied them to characterise the aggregation pathway of several disease-related proteins in vitro. In many such methodologies, the protein of interest needs to be tagged with either an organic fluorophore or a fluorescent protein. This is very challenging for in vivo or in cell imaging, and in some cases the label can have an adverse effect on the behaviour of the protein.^[15] Alternatively, dyes such as thioflavin-T/S (ThT/S) or the pentameric form of formyl thiophene acetic acid (pFTAA), whose fluorescence in each case is enhanced upon binding to amyloid structures, can be used to detect protein aggregates. We have recently used such dyes in combination with total internal reflection fluorescence (TIRF) microscopy to image individual aggregates in human cerebrospinal fluid (CSF) in a diffraction-limited manner.^[16] Such dyes, however, bind to other cellular components, thus limiting their versatility,^[17] and might not be sensitive to the smaller oligomers that, in addition to being major therapeutic targets, could also be biomarkers for neurodegeneration.^[16, 18] Furthermore, conventional far-field microscopy techniques face a limit in the resolving capability imposed by the optical diffraction barrier. As many subcellular structures are known to be affected by toxic protein aggregates,^[19, 20] it is

[a] D. R. Whiten,⁺ Y. Zuo,⁺ S. De, P. Flagmeier, D. C. Wirthensohn, F. Kundel, Dr. R. T. Ranasinghe, S. E. Sanchez, S. F. Lee, C. M. Dobson, D. Klenerman, M. H. Horrocks
Department of Chemistry, University of Cambridge
Lensfield Road, Cambridge CB2 1EW (UK)
E-mail: dk10012@cam.ac.uk

[b] D. Klenerman
UK Dementia Research Institute, University of Cambridge
Cambridge CB2 0XY (UK)

[c] L. Calo, M.-G. Spillantini
Department of Clinical Neurosciences, University of Cambridge
Hills Road, Cambridge CB2 0AH (UK)

[d] M.-L. Choi, D. Athauda, S. Gandhi
UCL Institute of Neurology
Queen Square, London WC1N 3BG (UK)

[e] M. H. Horrocks
Present addresses: EaStCHEM School of Chemistry, University of Edinburgh
David Brewster Road, Edinburgh EH9 3FJ (UK)
E-mail: mathew.horrocks@ed.ac.uk

[f] M. H. Horrocks
UK Dementia Research Institute, University of Edinburgh
Edinburgh (UK)

[*] These authors contributed equally to this work.

Supporting information and the ORCID identification numbers for the authors of this article can be found under <https://doi.org/10.1002/cbic.201800209>.

© 2018 The Authors. Published by Wiley-VCH Verlag GmbH & Co. KGaA. This is an open access article under the terms of the Creative Commons Attribution License, which permits use, distribution and reproduction in any medium, provided the original work is properly cited.

important to define the morphology and location of aggregates in the cellular milieu in order to understand the interplay between protein aggregation and the loss of cellular homeostasis.

We have used an aptamer previously reported to recognise oligomers and fibrils formed from α S and A β ^[21] to enable the sensitive and specific visualisation of protein aggregates at the nanoscale. Aptamers are single-stranded oligonucleotides developed to have high affinity and specificity and can be made for almost any molecule or structure.^[22,23] The advent of super-resolution (SR) microscopy^[24] has improved optical methods. Recently, an SR method, referred to as DNA PAINT (point accumulation in nanoscale topography), has been developed.^[25,26] The technique uses short complementary strands of DNA: a “docking” strand is conjugated to an antibody or a protein of interest, whilst its complementary “imaging” strand is labelled with an organic fluorophore. We extended the aptamer sequence with a docking strand sequence (Figure 1 A, Table S1 in

the Supporting Information) to generate SR images of protein aggregates (Figure 1 D); we refer to this method as aptamer DNA PAINT (ADPAINT). Repeated transient binding of the imaging strands to the docking strand (Figure 1 A–C) allows the labelled biomolecule to be spatially localised and enables the reconstruction of an SR image. Additional burst montages are shown in Figure S2 and provide a more complete view of the variation in fluorescent bursts caused by the stochastic binding of the imaging strands to the docking strand. DNA PAINT works with both TIRF microscopy and, more recently, spinning-disk confocal microscopy.^[27] Examples of both α S and A β oligomers and fibrils imaged by using ADPAINT are shown in Figure 1 D (full fields of view are shown in Figures S3 and S4). A control experiment on just the imaging strand (without aptamer) showed little nonspecific binding of the imaging strands to the aggregates (Figure S5). The aptamer is specific to the conformation of the aggregates, so these can be detected even amongst an excess of monomers. Furthermore, for primary and secondary antibodies, the size of a probe can add a linkage error of 15 nm,^[28] whereas the small size of aptamers enables them to bind at a higher density and at closer proximity to their epitopes; this leads to a higher imaging resolution, as has also been shown with DNA PAINT and non-antibody binding proteins such as affimers.^[29] Typically, we achieve a localisation precision of ≈ 10 nm and a resolution of ≈ 25 nm (Table S2), with a limit of detection of ≈ 30 pM of aggregates (see the Supporting Information). This enables us to quantify the oligomers formed during physiologically relevant aggregation reactions. Each image was acquired over 200 s; however, as PAINT-based techniques are not limited by photobleaching,^[30] this time can be lengthened to localise a greater number of binding events in order to obtain a higher-resolution image of the protein or the cellular structure of interest.

To assess the ability of ADPAINT to study the heterogeneity of complex aggregation mixtures, a solution of monomeric α S was incubated under conditions previously found to result in its aggregation.^[7,11] At early time points in the reaction, only a few aggregates were detected, and these were predominantly small (<400 nm in length for the first 6 h) and rounded; this is consistent with the expected appearance of oligomers (Figure 2 A). After 10 h, fibrils were detected. To visualise the distribution of binding sites within each aggregate, we colour-coded the localisations according to their local (typically within 40–50 nm) molecular density. The resulting images show maps of the local molecular density of individual aptamer binding sites, which reveal a highly non-uniform distribution, particularly in the later aggregates (right panel in each case). This shows that the aggregate structure is not homogeneous, but instead varies at the nanoscale, a finding that is made possible by this method. Further analy-

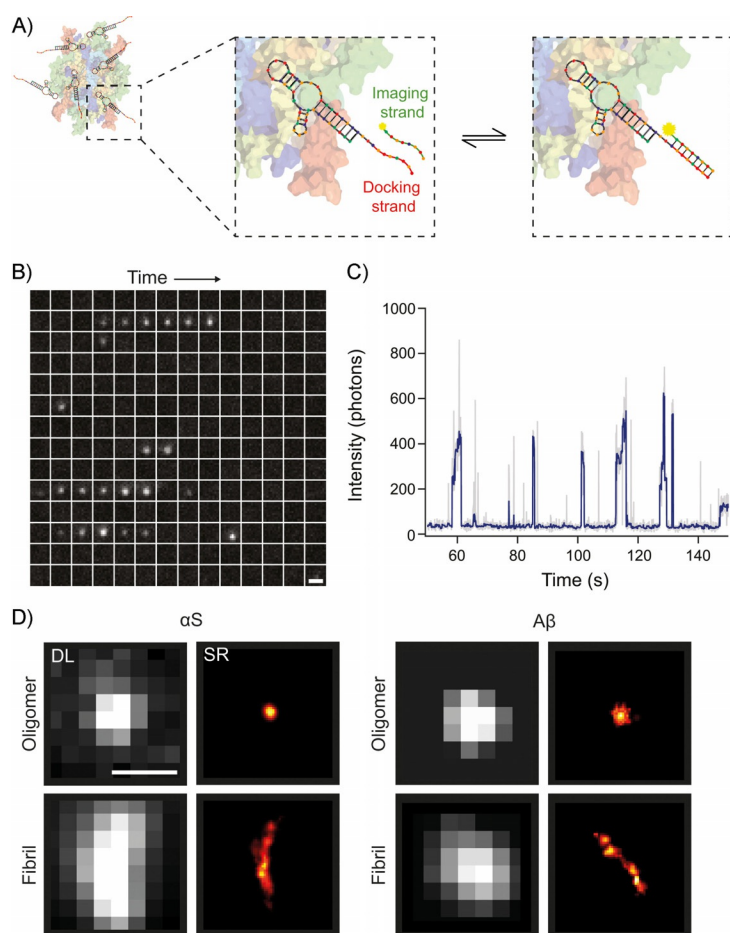


Figure 1. The concept of ADPAINT. A) Schematic representation of ADPAINT showing an aggregate bound by multiple aptamers. The DNA docking strand on the aptamer is transiently bound by the complementary imaging strand to generate a SR image. B) Example time montage of an oligomer undergoing ADPAINT. Each sub-image is separated by 0.5 s, moving through time from left to right then top to bottom; scale bar: 1 μ m. C) Intensity profile of the oligomer in (B). Each intensity burst represents the binding of the imaging strand to the aptamer. Grey: raw intensity profile, blue: using a Chung–Kennedy filter^[31] with a window of five frames applied. D) Examples of diffraction-limited (DL, using thioflavin-T) and super-resolved (using ADPAINT) images of an α S and A β oligomer and fibril. Scale bar: 500 nm.

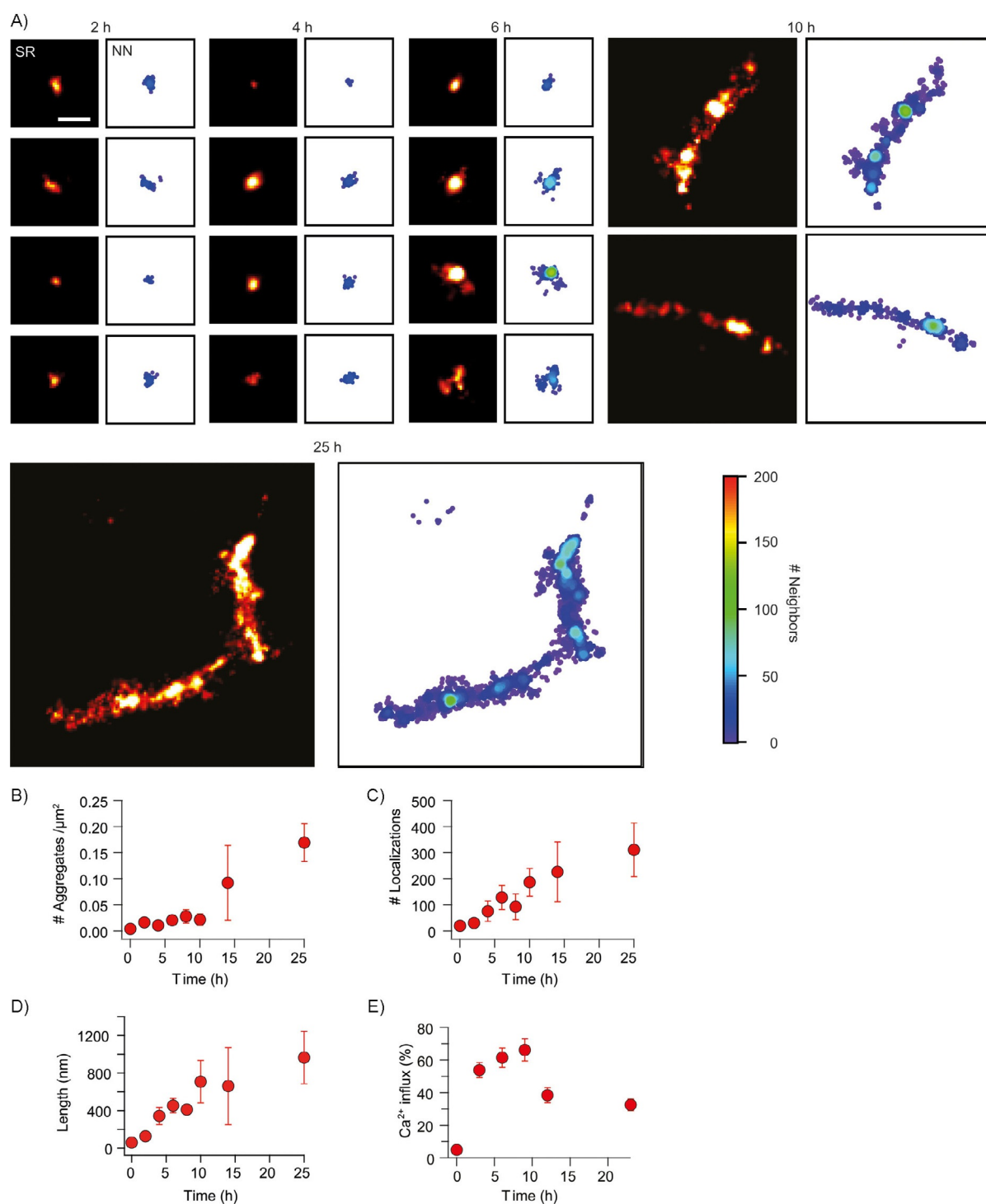


Figure 2. ADPAINT enables the imaging of a range of species formed during the aggregation of α S. A) Example aggregates are shown in SR on the left, with their corresponding nearest neighbour (NN) plots shown on the right, highlighting hotspots of localisation density. Scale bar: 200 nm. B) The number of aggregates increases over time, and C) the number of localisations also increases as the species get larger; this is shown by D) the mean length increases. Data shown are mean \pm SD of three independent aggregation reactions. E) The percentage of liposomes permeabilised upon addition of aggregates from the different time-points (mean \pm SD over 16 fields of view ($69 \times 69 \mu\text{m}$)).

sis of the ADPAINT images showed that the number of aggregates increased over time; this is consistent with the high aggregation propensity of α S (Figure 2B). Unlike antibodies in which stoichiometric labelling can be challenging, each apta-

mer is labelled with a single DNA docking strand, thus allowing quantitative imaging. We took advantage of this by quantifying the number of localisations per aggregate and found that this increased over time (Figures 2C and S6). Additionally, the

aggregates also became larger, as indicated by the increase in their mean length (Figures 2D and S7).

The permeabilisation of membranes has been suggested to be the most ubiquitous toxic mechanism associated with protein aggregates.^[31–35] We have developed a method to characterise the ability of protein aggregates to permeabilise lipid membranes^[8] (details are given in the Supporting Information) and applied it in this study. We found that the earlier aggregates caused a higher level of influx than those present at later stages of the aggregation process (those around 600 nm in length; Figure 2E). Additionally, the binding of the aptamer to the aggregates did not inhibit their ability to permeabilise the lipid membranes, and the aptamer itself displayed no propensity to alter these membranes (Figure S8). Thus, it appears likely that ADPAINT can be applied to characterise the structures of the pathological aggregates without altering the functional states of the protein or the cell membrane.

We next used ADPAINT to investigate aggregate formation in a cellular model of PD. Mis-sense mutations^[13,36–40] and duplications or triplications of the *SNCA* gene, which encodes α S, lead to autosomal dominant early onset PD.^[41,42] It has previously been shown that the formation of α S oligomers in vitro is concentration dependent,^[12] and ADPAINT now enables us to determine whether this dependence is reflected in cellular models that overexpress α S. We used induced pluripotent stem cells (iPSCs) from a PD patient with a triplication of the *SNCA* gene and from a healthy control unaffected by the disease to generate cortical neurons. Although SR methods have been used to image fibrils in cells, these are typically exogenously added aggregates generated from fluorophore-labelled protein.^[28,43–47] This is the first case in which a specific probe for aggregates has been used, and it enables the SR imaging of unlabelled, endogenous aberrant protein complexes. These were imaged in fixed, permeabilised cells by using both ADPAINT at the SR level and in a diffraction-limited manner by using pFTAA, a green dye that recognises β -sheet structures and becomes fluorescent upon binding to protein aggregates.^[48,49] To image at a greater depth into the cells, the illumination was changed from TIRF to oblique-angle epifluorescence. Figure 3 shows examples of human iPSC-derived neurons with and without the *SNCA* triplication after they have been plated and stained with pFTAA (further examples are shown in Figure S9). pFTAA not only binds to the aggregates, which appear as brighter spots, but also interacts with cellular organelles and membranes, thereby preventing the aggregates from being identified or their precise location within the cell from being determined. Unlike pFTAA, the aptamer has a high specificity, and only small clusters of binding events are detected within the cytosol. Due to the background fluorescence being higher in oblique-angle epifluorescence than in TIRF, the resolution we achieved within cells was lower than the resolution achieved for the aggregates formed in vitro (Table S2). Quantification of these images shows that there are significantly ($p < 0.0001$) more aggregates in the cells derived from the individual carrying a triplication of the *SNCA* locus compared to iPSC-derived neurons from the healthy control. We found that the species detected in these experiments resemble those formed early on in the in vitro aggregation pathway (0–2 h) shown in Figure 2, having ≈ 45 localisations per aggregate (Figure 3C), and being < 150 nm in length (Figure 3D). Furthermore, the aggregates detected in the cells having the *SNCA* triplication locus give rise to significantly more localisations (Figure 3C) and are larger (Figure 3D) than those in the healthy control cells. Given the likelihood of toxicity arising directly from these

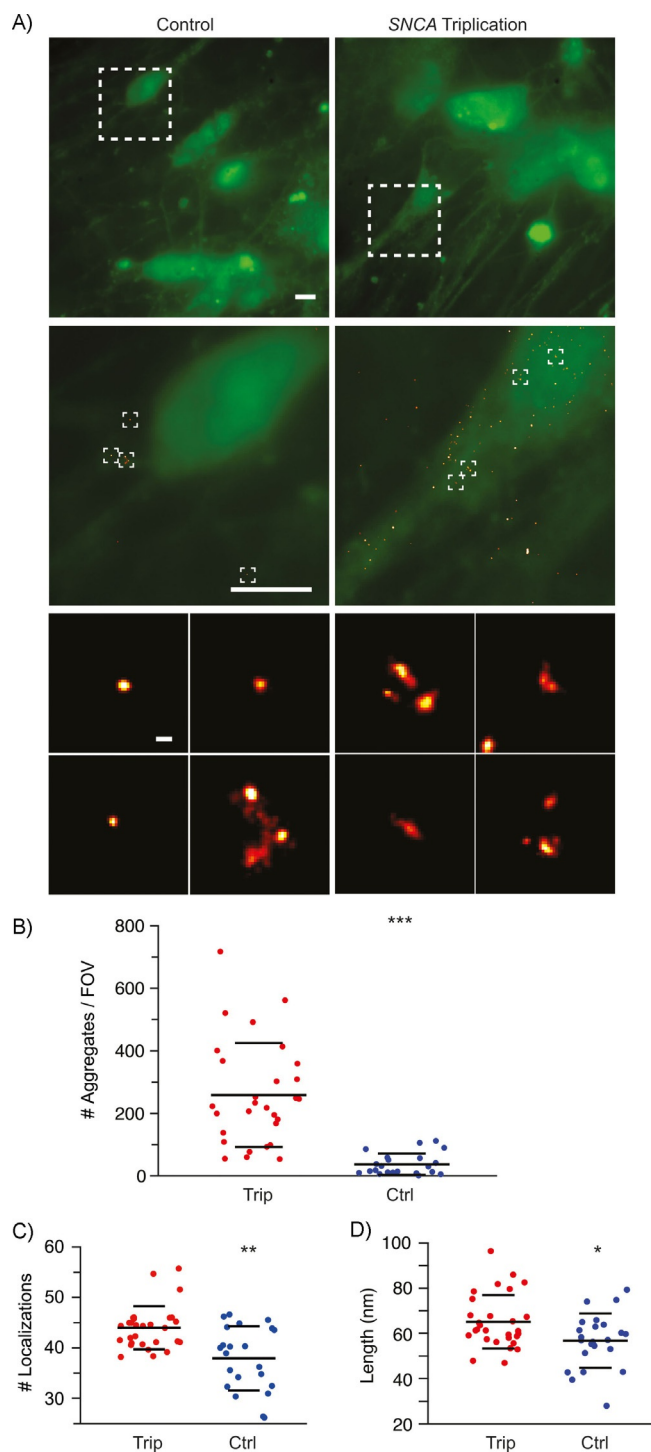


Figure 3. ADPAINT in iPSCs. A) iPSCs from a PD patient with a triplication of the *SNCA* gene and from a healthy control. Protein aggregates were imaged by using pFTAA (green) or ADPAINT (red). Scale bars: 5 μ m (top) and 100 nm (middle). Compared to control cells, *SNCA* triplication cells show B) significantly more aggregates and increases in C) the number of localisations and D) the average length of the aggregates. The data shown are means \pm SD of at least 27 fields of view. * $p < 0.05$, ** $p < 0.001$, *** $p < 0.0001$; analysed by t-test.

aggregates, this observation could help explain the neuronal cell death associated with PD.

One of the significant advantages of ADPAINT is the ability of the aptamer to selectively bind to protein aggregates but not the excess of monomeric protein that is present in cells. As a comparison, we used the commercially available MJF14-6-4-2 filament antibody, which detects an epitope that is only accessible in aggregates but not in the monomeric protein,^[50] and an Alexa Fluor 405-labelled aptamer to detect dual-labelled aggregates of α S added to iPSC-derived neurons (Figure S10). In the case of the MJF14-6-4-2 antibody, there was nonspecific staining of regions of the cell that did not contain aggregated α S, whereas the aptamer only detected dual-labelled aggregates. Furthermore, the larger size of antibodies can add a further 10–15 nm between the target and the labelled probe.^[28] When used with DNA PAINT, the same MJF14-6-4-2 antibody (Figure S11), was unable to resolve individual aggregates, but instead there was diffuse staining in both the SNCA triplication and control cells.

In conclusion, we have developed an SR method to characterise the toxic species formed during neurodegenerative diseases. We have used ADPAINT to characterise both in vitro aggregates α S and A β , as well as endogenous unlabelled oligomers formed in patient-derived neurons. Interestingly, we found that the aggregates formed early on in the in vitro aggregation closely resemble the morphology of those found within human iPSC-derived cortical neurons and that these appear to be most responsible for disrupting lipid membranes. Although only one stage in the lifetime of the iPSC-derived cortical neurons was imaged, this method can also be used to determine how such species develop as cells age, potentially yielding further insights into the progression of neurodegenerative diseases.

Acknowledgements

M.H.H. was supported by a Junior Research Fellowship at Christ's College, University of Cambridge, and the Herchel Smith Foundation. Y.Z. was supported by the Cambridge Trust and the Chinese Scholarship Council. P.F. was supported by Boehringer Ingelheim Fonds, and the German National Merit Foundation. S.D. is funded by a Marie-Curie Individual Fellowship. C.M.D. is supported by the Biotechnology and Biochemical Sciences Research Council and the Wellcome Trust. This work was also supported by the Cambridge Centre for Misfolding Diseases (P.F., and C.M.D.), the Royal Society (D.K.), the European Research Council with an ERC Advanced Grant (669237; D.R.W. and D.K.), and the Allen Distinguished Investigator Program, through The Paul G. Allen Frontiers Group (M.H.H.). M.G.S. and L.C. were supported by the Cambridge Biomedical Research Centre at Addenbrooke's Hospital, Cambridge and the Allen Foundation. The authors wish to thank Swapan Preet for purification of protein, and the mechanical workshops within the Department of Chemistry for aiding in the construction of single-molecule instrumentation.

Conflict of Interest

The authors declare no conflict of interest.

Keywords: amyloid formation · aptamers · DNA PAINT · induced pluripotent stem cells · neurodegenerative disorders · alpha-synuclein

- [1] F. Chiti, C. M. Dobson, *Annu. Rev. Biochem.* **2006**, *75*, 333–366.
- [2] S. Barghorn, P. Davies, E. Mandelkow, *Biochemistry* **2004**, *43*, 1694–1703.
- [3] M. G. Spillantini, M. L. Schmidt, V. M.-Y. Lee, J. Q. Trojanowski, R. Jakes, M. Goedert, *Nature* **1997**, *388*, 839–840.
- [4] P. J. Barrett, J. T. Greenamyre, *Brain Res.* **2015**, *1628*, 247–253.
- [5] H. Vicente Miranda, E. M. Szego, L. M. A. Oliveira, C. Breda, E. Darendelioglu, R. M. de Oliveira, D. G. Ferreira, M. A. Gomes, R. Rott, M. Oliveira, et al., *Brain* **2017**, *140*, 1399–1419.
- [6] A. Oueslati, M. Fournier, H. A. Lashuel, *Prog. Brain Res.* **2010**, *183*, 115–145.
- [7] N. Cremades, S. I. A. Cohen, E. Deas, A. Y. Abramov, A. Y. Chen, A. Orte, M. Sandal, R. W. Clarke, P. Dunne, F. A. Aprile, C. W. Bertoncini, N. W. Wood, T. P. J. Knowles, C. M. Dobson, D. Klenerman, *Cell* **2012**, *149*, 1048–1059.
- [8] P. Flagmeier, S. De, D. C. Wirthensohn, S. F. Lee, C. Vincke, S. Muyldermans, T. P. J. Knowles, S. Gandhi, C. M. Dobson, D. Klenerman, *Angew. Chem. Int. Ed.* **2017**, *56*, 7750–7754; *Angew. Chem.* **2017**, *129*, 7858–7862.
- [9] L. M. Billings, S. Oddo, K. N. Green, J. L. McLaugh, F. M. LaFerla, *Neuron* **2005**, *45*, 675–688.
- [10] R. M. Koffie, M. Meyer-Luehmann, T. Hashimoto, K. W. Adams, M. L. Mielke, M. Garcia-Alloza, K. D. Micheva, S. J. Smith, M. L. Kim, V. M. Lee, B. T. Hyman, T. L. Spire-Jones, *Proc. Natl. Acad. Sci. USA* **2009**, *106*, 4012–4017.
- [11] M. H. Horrocks, L. Tosatto, A. J. Dear, G. A. Garcia, M. Iljina, N. Cremades, M. Dalla Serra, T. P. J. Knowles, C. M. Dobson, D. Klenerman, *Anal. Chem.* **2015**, *87*, 8818–8826.
- [12] M. Iljina, G. A. Garcia, M. H. Horrocks, L. Tosatto, M. L. Choi, K. A. Gan-zinger, A. Y. Abramov, S. Gandhi, N. W. Wood, N. Cremades, C. M. Dobson, T. P. J. Knowles, D. Klenerman, *Proc. Natl. Acad. Sci.* **2016**, *113*, E1206–E1215.
- [13] L. Tosatto, M. H. Horrocks, A. J. Dear, T. P. J. Knowles, M. Dalla Serra, N. Cremades, C. M. Dobson, D. Klenerman, *Sci. Rep.* **2015**, *5*, 16696.
- [14] S. L. Shamma, G. A. Garcia, S. Kumar, M. Kjaergaard, M. H. Horrocks, N. Shivji, E. Mandelkow, T. P. J. Knowles, E. Mandelkow, D. Klenerman, *Nat. Commun.* **2015**, *6*, 7025.
- [15] V. L. Anderson, W. W. Webb, *BMC Biotechnol.* **2011**, *11*, 125.
- [16] M. H. Horrocks, S. F. Lee, S. Gandhi, N. K. Magdalinou, S. W. Chen, M. J. Devine, L. Tosatto, M. Kjaergaard, J. S. Beckwith, H. Zetterberg, et al., *ACS Chem. Neurosci.* **2016**, *7*, 399–406.
- [17] S. Sugimoto, K. Arita-Morioka, Y. Mizunoe, K. Yamanaka, T. Ogura, *Nucleic Acids Res.* **2015**, *43*, e92–e92.
- [18] T. Tokuda, M. M. Qureshi, M. T. Ardah, S. Varghese, S. A. S. Shehab, T. Kasai, N. Ishigami, A. Tamaoka, M. Nakagawa, O. M. A. El-Agnaf, *Neurology* **2010**, *75*, 1766–1772.
- [19] D. Snead, D. Eliezer, *Exp. Neurol.* **2014**, *23*, 292–313.
- [20] L. Ruan, C. Zhou, E. Jin, A. Kucharavy, Y. Zhang, Z. Wen, L. Florens, R. Li, *Nature* **2017**, *543*, 443–446.
- [21] K. Tsukakoshi, K. Abe, K. Sode, K. Ikebukuro, *Anal. Chem.* **2012**, *84*, 5542–5547.
- [22] C. Tuerk, L. Gold, *Science* **1990**, *249*, 505–510.
- [23] A. D. Ellington, J. W. Szostak, *Nature* **1990**, *346*, 818–822.
- [24] M. H. Horrocks, M. Palayret, D. Klenerman, S. F. Lee, *Histochem. Cell Biol.* **2014**, *141*, 577–585.
- [25] R. Jungmann, C. Steinhauer, M. Scheible, A. Kuzyk, P. Tinnefeld, F. C. Simmel, *Nano Lett.* **2010**, *10*, 4756–4761.
- [26] R. Jungmann, M. S. Avendaño, J. B. Woehrstein, M. Dai, W. M. Shih, P. Yin, *Nat. Methods* **2014**, *11*, 313–318.
- [27] F. Schueder, J. Lara-Gutiérrez, B. J. Beliveau, S. K. Saka, H. M. Sasaki, J. B. Woehrstein, M. T. Strauss, H. Grabmayr, P. Yin, R. Jungmann, *Nat. Commun.* **2017**, *8*, 2090.
- [28] S. J. Sahl, L. E. Weiss, W. C. Duim, J. Frydman, W. E. Moerner, *Sci. Rep.* **2012**, *2*, 895.

- [29] T. Schlichthaerle, A. S. Eklund, F. Schueder, M. T. Strauss, C. Tiede, A. Curd, J. Ries, M. Peckham, D. C. Tomlinson, R. Jungmann, *Angew. Chem. Int. Ed.* **2018**, *57*, 11060; *Angew. Chem.* **2018**, *130*, 11226.
- [30] A. Sharonov, R. M. Hochstrasser, *Proc. Natl. Acad. Sci. USA* **2006**, *103*, 18911–18916.
- [31] C. Soto, *Nat. Rev. Neurosci.* **2003**, *4*, 49–60.
- [32] C. Haass, D. J. Selkoe, *Nat. Rev. Mol. Cell Biol.* **2007**, *8*, 101–112.
- [33] I. Benilova, E. Karran, B. De Strooper, *Nat. Neurosci.* **2012**, *15*, 349–357.
- [34] M. Andreasen, N. Lorenzen, D. Otzen, *Biochim. Biophys. Acta Biomembr.* **2015**, *1848*, 1897–1907.
- [35] M. Serra-Batiste, M. Ninot-Pedrosa, M. Bayoumi, M. Gairí, G. Maglia, N. Carulla, *Proc. Natl. Acad. Sci. USA* **2016**, *113*, 10866–10871.
- [36] J. J. Zarranz, J. Alegre, J. C. Gómez-Esteban, E. Lezcano, R. Ros, I. Ampuero, L. Vidal, J. Hoenicka, O. Rodriguez, B. Atarés, V. Llorens, E. Gomez Tortosa, T. del Ser, D. G. Muñoz, J. G. de Yébenes, *Ann. Neurol.* **2004**, *55*, 164–173.
- [37] S. Lesage, M. Anheim, F. Letournel, L. Bousset, A. Honoré, N. Rozas, L. Pieri, K. Madiona, A. Dürr, R. Melki, C. Verny, A. Brice, *Ann. Neurol.* **2013**, *73*, 459–471.
- [38] P. Flagmeier, G. Meisl, M. Vendruscolo, T. P. J. Knowles, C. M. Dobson, A. K. Buell, C. Galvagnion, *Proc. Natl. Acad. Sci. USA* **2016**, *113*, 10328–10333.
- [39] M. H. Polymeropoulos, C. Lavedan, E. Leroy, S. E. Ide, A. Dehejia, A. Dutra, B. Pike, H. Root, J. Rubenstein, R. Boyer, E. S. Stenroos, S. Chandrasekharappa, A. Athanassiadou, Th. Papapetropoulos, W. G. Johnson, A. M. Lazzarini, R. C. Duvoisin, G. Di Iorio, L. I. Golbe, R. L. Nussbaum, *Science* **1997**, *276*, 2045–2047.
- [40] R. Krüger, W. Kuhn, T. Müller, D. Voitalla, M. Graeber, S. Kösel, H. Przuntek, J. T. Epplen, L. Schöls, O. Riess, *Nat. Genet.* **1998**, *18*, 106–108.
- [41] M.-C. Chartier-Harlin, J. Kachergus, C. Roumier, V. Mouroux, X. Douay, S. Lincoln, C. Levecque, L. Larvor, J. Andrieux, M. Hulihan, N. Waucquier, L. Defebvre, P. Amouyel, M. Farrer, A. Destée, *Lancet Lond. Engl.* **2004**, *364*, 1167–1169.
- [42] A. B. Singleton, M. Farrer, J. Johnson, A. Singleton, S. Hague, J. Kachergus, M. Hulihan, T. Peuralinna, A. Dutra, R. Nussbaum, et al., *Science* **2003**, *302*, 841.
- [43] G. S. Kaminski Schierle, S. van de Linde, M. Erdelyi, E. K. Esbjörner, T. Klein, E. Rees, C. W. Bertoncini, C. M. Dobson, M. Sauer, C. F. Kaminski, *J. Am. Chem. Soc.* **2011**, *133*, 12902–12905.
- [44] E. K. Esbjörner, F. Chan, E. Rees, M. Erdelyi, L. M. Luheshi, C. W. Bertoncini, C. F. Kaminski, C. M. Dobson, G. S. Kaminski Schierle, *Chem. Biol.* **2014**, *21*, 732–742.
- [45] M. J. Roberti, J. Fölling, M. S. Celej, M. Bossi, T. M. Jovin, E. A. Jares-Erijman, *Biophys. J.* **2012**, *102*, 1598–1607.
- [46] M. M. Apetri, R. Harkes, V. Subramaniam, G. W. Canters, T. Schmidt, T. J. Aartsma, *PLoS One* **2016**, *11*, e0153020.
- [47] D. Pinotsi, C. H. Michel, A. K. Buell, R. F. Laine, P. Mahou, C. M. Dobson, C. F. Kaminski, G. S. Kaminski Schierle, *Proc. Natl. Acad. Sci. USA* **2016**, *113*, 3815–3819.
- [48] J. Brelstaff, M. G. Spillantini, A. M. Tolkovsky, *Neural Regen. Res.* **2015**, *10*, 1746–1747.
- [49] J. Brelstaff, B. Ossola, J. J. Neher, T. Klingstedt, K. P. R. Nilsson, M. Goedert, M. G. Spillantini, A. M. Tolkovsky, *Front. Neurosci.* **2015**, *9*, 184.
- [50] L. B. Lassen, E. Gregersen, A. K. Isager, C. Betzer, R. H. Kofoed, P. H. Jensen, *PLoS One* **2018**, *13*, e0196056.

 Manuscript received: April 21, 2018

Revised manuscript received: July 8, 2018

Accepted manuscript online: July 27, 2018

Version of record online: September 11, 2018